Research Article

Bujagouni Karthik Goud, Dinesh Venkatesh Udupa, Chilakala Prathap, Deepak Dilip Shinde, Kompalli Divakar Rao* and Naba Kishore Sahoo

Noncontact three-dimensional quantitative profiling of fast aspheric lenses by optical coherence tomography

DOI 10.1515/aot-2016-0056
Received July 28, 2016; accepted November 10, 2016; previously published online December 19, 2016

Abstract: The use of optical coherence tomography (OCT) for noncontact three-dimensional aspheric lens profiling and retrieval of aspheric surface parameters is demonstrated. Two commercially available aspheric lenses with different focal length-to-diameter ratio have been imaged using OCT, and the measured optical path length distribution has been least square fitted with the aspheric lens surface retrieving the radius of curvature, aspheric constant, and conic constants. The refractive index of these lenses has also been measured referencing with a standard Zerodur glass flat. The fitted aspheric surface coefficients of the lenses are in close agreement with the manufacturer's values, thus, envisaging the potential of OCT in rapid screening, testing of aspheric lenses, and other micro-optical components such as those used in illumination optics.

Keywords: aspheric lens; aspheric surface; optical coherence tomography; refractive index.

***Corresponding author: Kompalli Divakar Rao,** Photonics and Nanotechnology Section, Atomic and Molecular Physics Division, BARC Facility, Visakhapatnam 530012, India, e-mail: divakar@barc.gov.in. http://orcid.org/0000-0002-8377-6765
Bujagouni Karthik Goud, Chilakala Prathap and Deepak Dilip Shinde: Photonics and Nanotechnology Section, Atomic and Molecular Physics Division, BARC Facility, Visakhapatnam 530012, India
Dinesh Venkatesh Udupa and Naba Kishore Sahoo: Atomic and Molecular Physics Division, Bhabha Atomic Research Centre, Trombay, Mumbai 400 085, India

1 Introduction

Optical coherence tomography (OCT) is a noncontact non-invasive biomedical optical imaging tool for various biomedical applications [1, 2]. OCT has been extremely successful in the field of clinical ophthalmology, and several applications are emerging rapidly for imaging other organs as well. Though OCT has been primarily a biomedical imaging tool, several non-medical applications have also been demonstrated using OCT. These include imaging crater depth in laser-induced damage in optical materials, depth-resolved imaging of microstructures in composite materials, strain mapping of reinforced composites, and so on [3]. Recently, OCT has been demonstrated for noncontact profilometric applications of metallic surfaces with high accuracy compared to a conventional two-beam interferometer [4]. In addition, OCT has also been used for precision measurement of refractive index of materials. Gradient in refractive index is widely used in optical industry in GRIN lenses, GRIN fibers, etc. A quantitative measurement of such gradient in refractive index profile is crucial for evaluating such components. The Graded Index (GRIN) lenses are common feature in visual systems as well. Aquatic animals like fish have spherical gradient index lenses. Verma et al. [5] demonstrated for the first time refractive index profile of crystalline lens of fish eye *in vivo* using OCT. Work on profiling of human crystalline lens and estimation of its asphericity was reported by Ortiz et al. [6]. Lv et al. [7] have used OCT for non-destructive measurement of index profile of GRIN rod lenses by iterative fitting of optical paths calculated by ray tracing. Yao et al. [8] developed swept source-based angular scanned OCT system for imaging polymeric GRIN performs.

While spherical optics is easy to design and manufacture, it has greater limitations in aberration correction in an optical system compared to aspherics. Often, several spherical lenses are replaced by a single aspheric in an

optical system for a similar or even improved optical performance resulting in reduced complexity and weight. In the recent times, aspheric lenses are increasingly being used in optical systems with wide ranging applications such as in LED collimators [9], etc. In view of the heavy production volume of aspherics, there has been recent focus on devising tools for rapid evaluation of aspheric surface and its characterization with high precision. Conventionally, null tests have been employed for testing aspherics where near-perfect plane or spherical wavefronts resulting from optical arrangements with the aspheric are tested against plane or spherical standards interferometrically [10]. Several techniques and improvements relating to null tests for aspherics have been reported in the literature such as the use of dynamic membranes [11], digital phase-shifting interferometry [12], sub-aperture stitching interferometry [13], and null Ronchi test [14] to name a few. Other testing techniques include using null element computer-generated holograms [15], Shack-Hartmann sensors [16], simple ray tracing methods [17], deflectrometric methods [18], and fringe reflection photogrammetry [19]. However, most of these methods are suitable for low-aperture and large-sized optics. Some other techniques for deeply curved aspheric testing mentioned in the literature include synthetic aperture interferometry, which is based on aperture scanning interferometry [20] and sub-aperture stitching interferometry [21] combining many sub-aperture data. These aim to overcome the limitations of full aperture interferometric techniques in deep aspheric testing such as high fringe density and vignetting. Sun et al. [22] have developed a new approach for three-dimensional fitting of aspheric data based on nonlinear least-squares algorithm. Hayeka et al. have proposed new algorithms for form characterization of aspherical surfaces for large-scale volume data sets [23]. Another technique based on confocal spectral interferometry is implemented in commercially available metrology systems for aspheric shapes [24].

Laser Fizeau interferometer employing the null optical arrangement is conventionally used as an effective technique for aspheric shape error measurements. However, some drawbacks in this technique are inherent to the null method itself. While null optical techniques can be used for measuring fast aspherics with deep curvatures, null optic components are required to be tested and qualified, themselves, and are often expensive. Besides, a null optical component is specific to the aspheric being tested. The interferometric method is also very sensitive to the optical alignment and the positioning of test surface.

Recently, metrology for free-form shapes based on OCT using swept source scanning has been demonstrated for 400-μm surface sag with a maximum slope of 5 arc-degrees [25]. In this paper, we demonstrate a new application of OCT for noncontact three-dimensional depth profiling of fast (deeply curved) aspheric lenses available off the shelf from commercial suppliers. The non-requirement of null optical elements in the OCT technique is advantageous compared to the interferometric methods. OCT technique can also be used for surface profile measurements of partially polished or rough surface in the pre-polishing stages, as the method relies on the backscattered light from the surface. In our work, three-dimensional optical path length data from OCT has been used to iteratively fit aspheric surfaces to retrieve conic constants, aspheric coefficients, and radius of curvature. In addition, we also estimate the refractive index of the lens. The fitted values closely match with the manufacturer's values within the experimental errors for two commercial lenses.

2 OCT experimental setup

Figure 1 shows a schematic of time domain OCT system. Light from a superluminescent diode (SLD, Dense Light, Singapore) with a center wavelength of ~ 830 nm and bandwidth 30 nm is coupled to a 2×2 fused fiber optic single-mode fiber coupler with 50/50 splitting ratio. Light from one path (reference arm) is collimated and coupled to a reference mirror mounted on a motorized translation stage (Holmarc, India). The reference mirror stage is repeatedly scanned back and forth with a uniform speed for generating time delay. Light from the other path (sample arm) is collimated and passed through a 10× microscopic objective [Newport, M10X, focal length ~16.5 mm, numerical aperture (NA) ~0.25]. The sample aspheric lens is placed at the focal plane of the objective lens and is mounted on another motorized stage for generating lateral scanning.

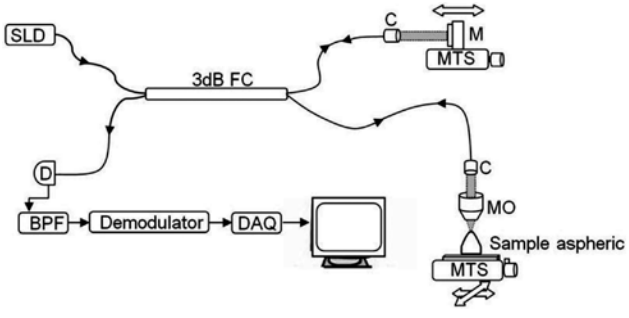

Figure 1: Schematic of time domain optical coherence tomography (OCT) system. BPF, Band pass filter; C, collimator lens; D, photodiode; DAQ, data acquisition card; FC, fiber coupler; MO, microscopic objective; MTS, motorized translation stage; SLD, superluminescent diode.

The light reflected from both the sample and reference arms is collected by a photoreceiver whose output is band pass filtered and fed to a lock-in amplifier for demodulating the interferometric signal. A data acquisition board (National Instruments PCI 6110) digitized the demodulated interferometric signal. The reference arm scan generates the axial (depth-resolved) profiles of the sample termed as A-scans along the Z direction. Lateral scanning of the sample by two translation stages (moved in XY plane) is used to generate A-scans at different lateral positions over the test lens. A-scans at different Y positions of the sample aspheric for a fixed X position generates two-dimensional cross-sectional images in the YZ plane. The position of the sample aspheric is also varied in the X direction by another translation stage for acquiring three-dimensional tomographic data. The setup is controlled using LabVIEW for obtaining two-dimensional cross-sectional images. The axial (depth) resolution of the system is estimated to be ~11 μm by measuring the full width half maximum of the autocorrelation envelope when the sample aspheric is replaced by a high-reflecting mirror. The lateral resolution of the system is given by the focal spot size on the sample, which is estimated to be ~20 μm. As the reference plane of the measurement in the system is defined by the scanning plane (XY plane), the planarity of the XY stage determines the accuracy limit. This was ascertained to be less than one step (11 μm) by measuring the surface shape of a standard optical flat (flatness ~λ/10) across a scan of 50-mm length. SNR (signal-to-noise ratio) of the TD-OCT setup is ~95 dB at incident power of 1.5 mW, when high-reflecting mirror was used as a sample.

3 Shape measurement of aspheric lens

The test aspheric lens samples consisted of lenses with two different aspheric curvatures from Thorlabs, USA (www.thorlabs.com) for imaging with OCT. These are plano-convex Thorlabs model ACL1815 (focal length 15 mm and diameter 18 mm) and ACL1210 (focal length 10 mm and diameter 12.5 mm) made of B270 Superwite® glass. The lens ACL1815 has an aspheric surface with a sag of 4.48 mm and a maximum surface slope of 51.8°, whereas the lens ACL1210 has an aspheric surface with a sag of 3.88 mm and a maximum surface slope of 88.7°. As the aim is to measure the full shape of the lens and not to image any microstructures in the lens, we have taken lateral scanning steps somewhat higher than the focal spot size. For example, for imaging 10-mm focal length aspheric lens, we have taken 500 lateral scans over 15-mm range giving a lateral step of 30 μm. For imaging 15-mm focal length aspheric lens, we have acquired 500 scans over 20 mm in the lateral direction giving a lateral step of 40 μm. For three-dimensional tomographic data, about 20 YZ cross-sectional images have been acquired, in the X direction with a typical step of 0.75 mm.

An aspheric surface can be mathematically expressed as a departure from a spherical surface by the equation [26]

$$z = \frac{c\rho^2}{1+\sqrt{1-(1+k)c^2\rho^2}} + A_4\rho^4 + A_6\rho^6 + \ldots \quad (1)$$

where $\rho^2 = (x^2 + y^2)$

Here, x, y, z are the surface coordinates with z being in the longitudinal direction and y in the lateral direction and $(x, y, z) = (0, 0, 0)$ at the pole of the aspheric. Also, c is the curvature, k is the conic constant, and A_4 and A_6 are the aspheric constants. The coordinates of the various surface points acquired in the experiment is fitted to the surface equation (1) by nonlinear least square fitting to obtain the best-fit values of c, k, and A_4. We have used the Newton-Gauss method as the fitting algorithm for the nonlinear least square fitting and obtained a convergence in 10 and 14 iterations for ACL1815 and ACL 1210 lens surface, respectively. The expected values of the parameters from the manufacturer's data sheet were chosen as the initial estimate. The standard errors in the parameters obtained in the fitting indicate the range of these parameters, which will still result in the same overall residual error in the fit and can be taken as uncertainties in the determination of the parameters. A few clearly noisy data points of the surface, which occur due to saturation of demodulation in the signal acquisition, environmental disturbances, etc., had to be eliminated for the fitting.

Figure 2 shows the OCT images of the aspheric lens ACL1815 with the probe beam incident from the top. In Figure 2A, the aspheric surface of the lens is on the top side facing the probe beam. The bottom profile is the flat surface as imaged through the lens. Figure 2B shows the

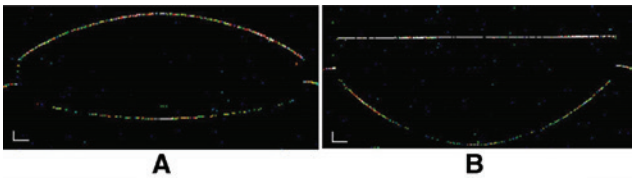

Figure 2: OCT images of aspheric lens (ACL1815) with probe beam incident from the top. (A) Aspheric surface on top facing the probe beam and (B) flat surface on top facing the probe beam. The scale bar shown at the bottom of the image is 1 mm.

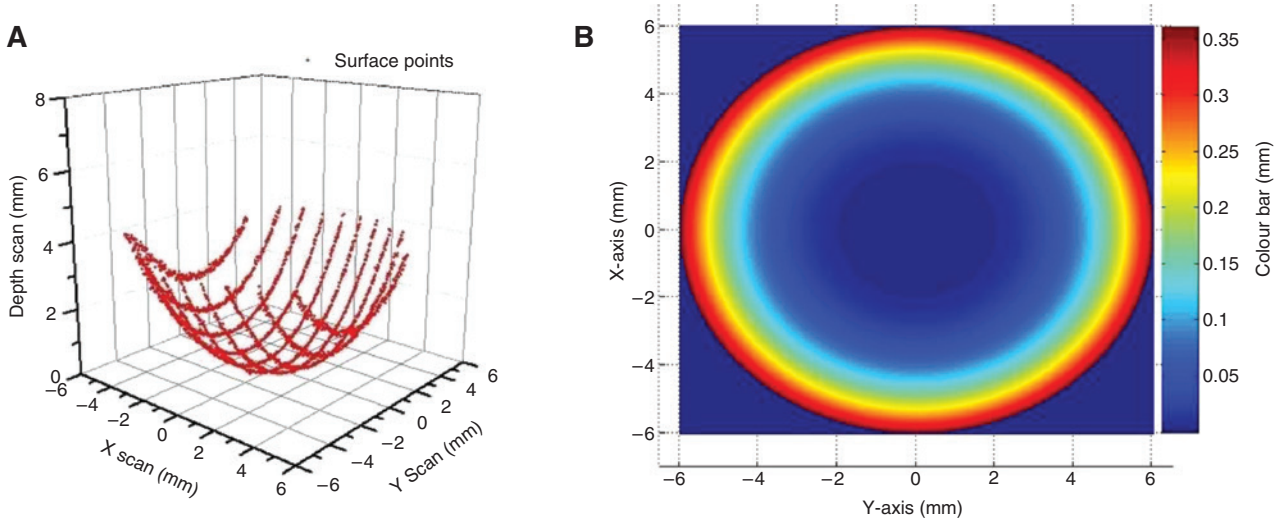

C

Model	Aspheric 1 (User)		
Equation	$z=c*((x-a1)^2+(y-a2)^2)/(1+\sqrt{1-(1+k)*((x-a1)^2+(y-a2)^2)*c^2})+b+m*((x-a1)^2+(y-a2)^2)^2$		
Reduced Chi-Sqr	0.00328		
Adj. R-Squa	0.99702		
		Value	Standard error
X centre	a1	−0.07207	0.00166
Y centre	a2	−0.0427	0.00141
Curvature	c	0.18217	0.00188
Conic	k	−0.71254	0.0561
Z shift	b	0.02858	0.00393
A4	m	4.74155E-4	6.391E-5

Figure 3: (A) Three-dimensional plot of the surface data points acquired for the lens ACL1210. (B) Plot of surface form deviation with respect to the nominal designed value for the lens ACL1210. (C) Table indicating the fitted aspheric surface parameters.

OCT image of the same lens with a flat surface on the top side facing the probe beam.

The scans of Figure 2 are taken along a line passing through the lens center. Figure 3A shows the three-dimensional plot of the surface data points acquired for the lens ACL1210 using the setup with the convex aspheric surface facing the probe beam along with the parameters obtained by surface fitting (shown in Figure 3C). The surface form deviation is defined as the departure of the actual surface of the lens from the ideal (designed) aspheric form. Quantifying form deviation can be used to improve surface profile closer to the ideal aspheric form in fabrication of aspherics. Figure 3B shows the surface form deviation with respect to the nominal designed value for the lens ACL1210. Form deviation was obtained by the difference between the profiles computed from fitted aspheric coefficients of the experimental data and that from manufacturer's aspheric constants. Figure 4A shows the 3-dimensional plot of the surface data points acquired for the lens ACL1815 using the setup with the convex aspheric surface facing the probe beam along with the parameters obtained by surface fitting (shown in Figure 4C). Figure 4B shows the surface form deviation with respect to the nominal designed value for the lens ACL1815. Note that the form deviation shown in Figures 3B and 4B is not the error in the measurement of the surface profile. Table 1 shows the comparison of the obtained parameters with respect to the manufacturer's values for the two lenses. Tables 2 and 3 show the measured surface parameters for the lens ACL1210 and the lens ACL1815, respectively, according to the ISO 10110-5 format.

4 Refractive index measurements

As can be seen in Figure 2, the technique also measures the optical path of the second surface of the lens from the top surface and can be used for determining the refractive index of the lens. However, as a low coherence light having a band of wavelength is used as the source, the optical path measured corresponds to group refractive index and not phase refractive index [27].

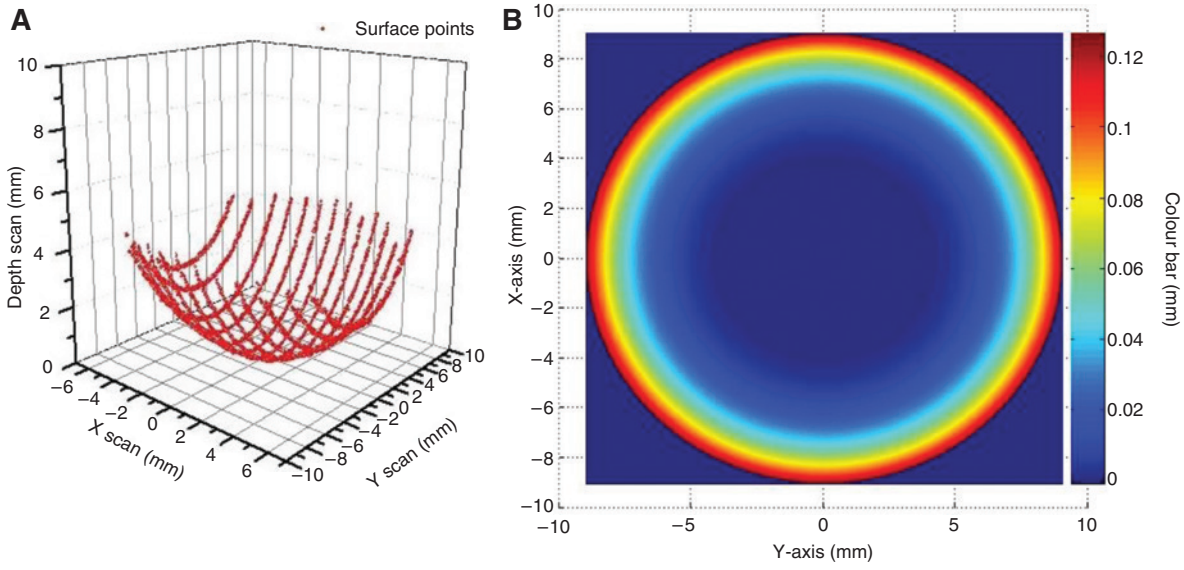

C

Model	Aspheric 1 (User)		
Equation	$z=c*((x-a1)^2+(y-a2)^2)/(1+sqrt(1-(1+k)*((x-a1)^2+(y-a2)^2)*c^2))+b+m*((x-a1)^2+(y-a2)^2)^2$		
Reduced Chi-Sqr	0.02774		
Adj. R-Sq	0.98017		
		Value	Standard error
X centre	a1	−0.24002	0.0062
Y centre	a2	−0.05492	0.00472
Curvature	c	0.126	0.00165
Conic	k	−0.63654	0.05764
Z shift	b	−0.01567	0.00833
A4	m	−1.96357E-4	3.791E-5

Figure 4: (A) Three-dimensional plot of the surface data points acquired for the lens ACL1815. (B) Plot of surface form deviation with respect to the nominal designed value for the lens ACL1815. (C) Table indicating the surface fitting parameters.

Table 1: Experimentally fitted aspheric lens parameters and manufacturer's values for two different aspheric lenses.

Parameter	Lens ACL1815			Lens ACL1210		
	Manufacturer's value	Experimental value	Standard error	Manufacturer's value	Experimental value	Standard error
C (mm^{-1})	0.12650	0.1260	0.00165	0.18207	0.18217	0.00188
K	− 0.675762	− 0.63654	0.0576	− 0.623014	− 0.71254	0.0561
A_4 (mm^{-1})	-2.0269×10^{-4}	-1.96×10^{-4}	3.79×10^{-5}	8.7×10^{-5}	4.74×10^{-4}	6.39×10^{-5}

Table 2: Experimentally measured surface parameters for the lens ACL1210 (as per ISO 10110-5 format).

Aperture (h) (mm)	Sag (Z) (mm)	Sag deviation (ΔZ) (mm)	Slope (S) (degree)	Slope deviation (ΔS) (degree)
0	0	–	0	–
1	0.09	0.0003	10.60	0.08
2	0.38	0.0052	22.15	0.59
3	0.88	0.0257	35.68	1.93
4	1.64	0.0790	52.31	4.38
5	2.73	0.1855	73.38	7.99

Table 3: Experimentally measured surface parameters for the lens ACL1815 (as per ISO 10110-5 format).

Aperture (h) (mm)	Sag (Z) (mm)	Sag deviation (ΔZ) (mm)	Slope (S) (degree)	Slope deviation (ΔS) (degree)
0	0	–	0	–
1	0.06	0	7.20	– 0.025
2	0.25	– 0.0007	14.25	– 0.028
3	0.56	– 0.0009	21.03	0.015
4	0.98	0.0002	27.44	0.133
5	1.51	0.0043	33.41	0.366
6	2.15	0.0140	38.96	0.771
7	2.87	0.0328	44.26	1.445
8	3.69	0.0669	49.72	2.560
9	4.61	0.1268	56.28	4.474

The group refractive index (n_g) is calculated as the ratio of the optical path length to the geometrical thickness:

$$n_g = \frac{D}{t} \tag{2}$$

where D is the optical thickness at the center of the lens, and t is the corresponding physical thickness. The error estimates in this calculation can be made by differentiating equation (2). If the errors in the D and t values are δD and δt, respectively, the maximum error in determining n_g will be

$$\frac{|\delta(n_g)|}{n_g} = \frac{|\delta D|}{D} + \frac{|\delta t|}{t} \tag{3}$$

where $\delta(n_g)$ is the maximum error in the group index.

The phase refractive index can then be obtained by the relation given by [28]:

$$n_p - \lambda_0 \frac{dn_p}{d\lambda_0} = n_g \tag{4}$$

where n_p and n_g are the phase refractive index and the group refractive index at the wavelength λ_0, respectively.

4.1 Verification using Zerodur® standard

The method for determining the group refractive index has been verified using a standard parallel plate of Zerodur® glass (SCHOTT) with a thickness of 12.55 ± 0.002 mm having a parallelism of 10 arc-sec. Figure 5 is the plot of the OCT data obtained by scanning the Zerodur plate showing the surface points of the Zerodur top surface, glass base plate, and the Zerodur bottom surface.

The optical thickness measured is 19.44 ± 0.024 mm giving a group refractive index of $n_g = 1.5490 \pm 0.002$

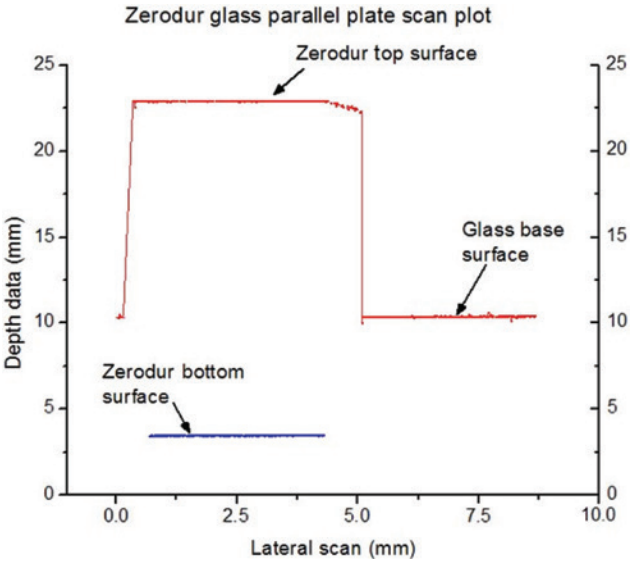

Figure 5: A plot of the data obtained from the OCT depth profile for a Zerodur® glass parallel plate showing the various surfaces.

from equation (2). The dispersion of Zerodur at 830 nm is -0.02 μm^{-1} resulting in the phase refractive index of $n_p = 1.5324 \pm 0.002$ from equation (4). The value is in close agreement with the value of 1.5346 in the SCHOTT glass catalog:

[http://www.schott.com/advanced_optics/english/download/schott_tie43_properties_of_zerodur_eng.pdf].

4.2 Refractive index of the aspheric lens

Estimation of the refractive index of the aspheric lens is done using OCT data obtained at the center of the lens. As the lens is not a graded index lens, refractive index is measured at the center as it has the highest optical path length. Considering the lens ACL1815, the optical path

difference between the front surface and the back surface of the aspheric lens at the center of lens (D) is 10.896 mm. The physical thickness at the center of the lens (t) is 7.1 mm. The group index from equation (2) is calculated as 1.5346 at 830 nm wavelength. In order to determine the phase refractive index of the lens, the dispersion ($dn_p/d\lambda_0$) for the B270 Superwite glass at $\lambda_0 = 830$ nm is found out from the dispersion curve for this glass plotted using the refractive indices at other wavelengths available in the literature [http://www.jnsglass.com/pdf/B270.pdf]. The dispersion curve of the B270 Superwite glass is shown in Figure 6.

The Sellmeier equation for dispersion is given by:

$$n^2(\lambda) - 1 = \frac{A_1\lambda^2}{\lambda^2 - B_1} + \frac{A_2\lambda^2}{\lambda^2 - B_2} + \frac{A_3\lambda^2}{\lambda^2 - B_3} \tag{5}$$

The values of the Sellmeier coefficients for the B270 Superwite glass obtained from the fitting of Figure 6 are:

$A_1 = 1.27457$; $B_1 = 0.01071\ \mu m^2$; $A_2 = 0.09101$; $B_2 = -1.94057\ \mu m^2$; $A_3 = -5229$ and $B_3 = -186{,}611\ \mu m^2$.

Hence, from the refractive index data for a few wavelengths available in the literature, the phase index n_p at 830 nm is found to be 1.5163, whereas the dispersion at $\lambda = 830$ nm is $(dn_p/d\lambda_0) = -0.01760122\ \mu m^{-1}$.

The experimental phase refractive index (n_p) for the lens ACL1815 is 1.520 ± 0.005 using Eq. (4). Similarly, the phase refractive index for the lens ACL1210 is derived to be 1.521 ± 0.006. The maximum error in the estimation of the optical path length (δD) is 0.018 mm. The maximum error in the estimation of the physical thickness (δt) is 0.01 mm, which is the least count of the screw gauge micrometer

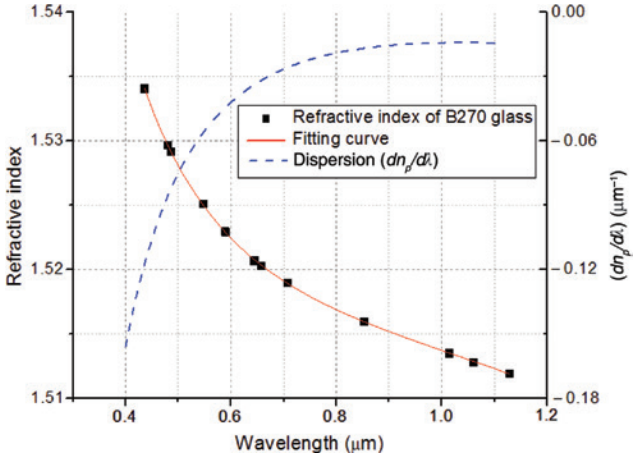

Figure 6: The refractive index and dispersion for the B270 Superwite glass from the refractive indices at various wavelengths taken from the literature.

Table 4: Experimentally measured group and estimated phase refractive indices of two aspheric lenses.

Aspheric lens	ACL1815	ACL1210
Physical center thickness (t)	7.1 ± 0.01 mm	5.87 ± 0.01 mm
Optical center thickness (D)	10.896 ± 0.018 mm	9.00 ± 0.018 mm
Group index at 830 nm (n_g)	1.5346 ± 0.005	1.5332 ± 0.006
Phase index at 830 nm (n_p)	1.520 ± 0.005	1.521 ± 0.006

used for the measurement. The errors in estimation of the group index $\delta(n_g)$ calculated using equation (3) are 0.005 and 0.006 for the lenses ACL1815 and ACL1210, respectively. The refractive index as measured from the OCT data for the two lenses are summarized in Table 4.

5 Accuracies of shape measurements

Repeatability of the optical path length measurements for our custom-built OCT setup was studied using the standard Zerodur glass parallel plate of thickness 12.55 ± 0.002 mm. Thirty-four successive axial scans were performed on the Zerodur plate at the same spot, and the standard deviation of the optical path length of Zerodur glass plate was found to be 18 μm.

Similarly, to estimate the errors contributed by the translational stage toward the optical path length measurement, the Zerodur glass plate surface was scanned by the setup, and the optical path difference between two surfaces of the Zerodur plate was obtained at 100 nearby points. The standard deviation of the data was found to be 18 μm. The error in the optical path length measurement using our set up is 18 μm.

Finally, we estimate the accuracies involved in the determination of aspheric coefficients. In order to estimate the error in the determination of c and k from the surface coordinate measurements, consider the equation defining a conic surface of revolution along the z axis

$$\rho^2 - 2rz + (k+1)z^2 = 0 \tag{6}$$

where we use polar coordinates (ρ, θ) to define a point over the aperture with $\rho^2 = x^2 + y^2$; $x = \rho\cos\theta$; $y = \rho\sin\theta$, and r is the radius of curvature with $r = \frac{1}{c}$.

The relations between small variations in the parameters can be written down by partially differentiating equation (6) as

$$2\rho\,\delta\rho - 2r\,\delta z - 2z\,\delta r + 2z(k+1)\,\delta z + z^2\,\delta k = 0 \tag{7}$$

Rearranging the terms, we get

$$z\delta r - \frac{z^2}{2}\,\delta k = \rho\,\delta\rho + (z(k+1) - r)\delta z \tag{8}$$

If $\delta\rho$ and δz are the small uncertainties in the position coordinates on the surface, then δr and δk are the uncertainties in the radius of curvature and the conic constant of the surface, respectively. The values of δx and δy are the accuracies of the translation stage displacements in the x and y directions, respectively, which in our case is $\delta x = \delta y = 0.01$ mm.

As $\delta\rho = \delta x\cos\theta + \delta y\sin\theta$, we can write in the present case,

$$\delta\rho = \delta x(\cos\theta + \sin\theta), \tag{9}$$

the maximum value of $\delta\rho$ is $\delta\rho\big|_{\max} = \sqrt{2}\,\delta x$ for $\theta = \pi/4$.

For the measurement on lens ACL1815, the minimum step size in the z direction was $\delta z = 0.02$ mm. If we substitute the values of the various parameters for this measurement as $\rho = 9.0$ mm; $z = 4.7$ mm; $r = (1/c) = 7.905$ mm; $k = -0.675762$ and $\delta\rho = 0.014$ mm, the maximum value of the left hand side of equation (8) is 0.338 mm^2.

For a rough estimation of the errors in r and k, we first assume that $\delta k = 0$ so as to get the maximum possible uncertainty in r as $\delta r = 0.0719$ mm, resulting in uncertainty in c as $\delta c = 0.0011$ mm^{-1}.

Similarly, assuming $\delta c = 0$, we get the maximum uncertainty in the conic constant k as $\delta k = 0.0306$.

The uncertainties in the experimentally determined values of c and k from the least square fit of the coordinate data points of the surface can be considered to be the standard errors for these parameters in the fitting. The standard error in the least square fit of the data gives $\delta c = 0.00165$ mm^{-1} and $\delta k = 0.0576$. The experimental values are in the same orders of magnitude as roughly estimated theoretical values.

6 Conclusion

To summarize, we have demonstrated the use of OCT for noncontact three-dimensional profiling of two commercially available deeply curved aspheric lenses (ACL1210 and ACL1815) from Thorlabs, USA. The surface shape parameters viz., radius of curvature, conic constant, and aspheric constant have been retrieved from the measured optical path length OCT data using two-dimensional nonlinear least squares fitting. The data is used for measuring the form deviation with respect to the manufacturer-specified values. The measured group refractive index and estimated phase index of these lenses have also been determined after validating the method with a standard reference plate of Zerodur® glass. The index values compare very well for the B270 Superwite glass material used in the lenses. Error analysis has been carried out to express the relative accuracies of the aspheric coefficients and refractive index of the lenses by this method. In this work, we have used a conventional time domain OCT system, which essentially demonstrates the proof of principle of aspheric shape and index measurement for fast aspherics. The accuracy of technique can be further improved using current state-of-the-art OCT systems offering resolutions of ~1–3 μm resulting in better accuracies, which may be comparable to that of the measurements carried out using contact-type coordinate measuring machines (CMM). The speed of our TD-OCT system is 1 axial scan per second at full reference arm sweep of 24 mm. However, with the state-of-the-art OCT systems, high data acquisition (axial scans at a few hundred kHz rate) is possible [29].

To the best of our knowledge, this is the first application of OCT demonstrating the noncontact quantitative metrology of fast aspheric with potential applications for rapid screening of micro-aspheric optics and related applications. Considering the accuracy of the measurements, this method can provide fast measurements for low-end aspherics such as illumination optics. Current OCT technology with real-time volumetric imaging OCT systems may soon find utilization in aspheric lens industry for routine metrological applications.

References

[1] A. F. Fercher, Z. Med. Phys. 20, 251–276 (2010).
[2] A. Gh. Podoleanu, J. Microsc. 247, 209–219 (2012).
[3] D. Stifter, Appl. Phys. B: Lasers Opt. 88, 337–357 (2007).
[4] K. Divakar Rao, D. V. Udupa, C. Prathap, A. Rathod, R. Balasubramaniam, et al. Opt. Lasers Eng. 66, 204–209 (2015).
[5] Y. Verma, K. D. Rao, M. Suresh, H. S. Patel and P. Gupta, Appl. Phys. B 87, 607–610 (2007).
[6] S. Ortiz, D. Siedlecki, I. Grulkowski, L. Remon, D. Pascual, et al. Opt. Express 18, 2782–2796 (2010).
[7] H. Lv, A. Liu, J. Tong, X. Yi, Q. Li, et al. Rev. Sci. Instrum. 81, 103104 (2010).
[8] J. Yao, P. Meemon, M. Ponting and J. P. Rolland, Opt. Express 23, 6428–6443 (2015).
[9] R.-S. Chen, Appl. Opt. 53, H129–H139 (2014).
[10] J. D. Briers, Opt. Lasers Eng. 32, 111–138 (1999).
[11] C. Pruss and H. J. Tiziani, Opt. Commun. 233, 15–19 (2004).
[12] G. Kang, J. Xie, P. Su, Q. Tan and G. Jin, Optik 121, 1586–1590 (2010).
[13] M. Tricard, A. Kulawiec, M. Bauer, G. DeVries, J. Fleig, et al., CIRP Ann. – Manuf. Technol. 59, 547–550 (2010).

[14] C. Guo, X. Su, W. Chen, B. Lei and F. Wu, Appl. Opt. 51, 1276–1282 (2010).
[15] S. Reichelt, C. Pruss and H. J. Tiziani, Appl. Opt. 42, 4468–4479 (2003).
[16] M. Rocktaschel and H. J. Tiziani, Opt. Laser Technol. 34, 631–637 (2002).
[17] H. Wang, Y. Li, L. Zeng, C. Yin and Z. Feng, Opt. Commun. 232, 61–68 (2004).
[18] Q. Hao, Opt. Laser Technol. 37, 375–380 (2005).
[19] Y. Xiao, X. Su, W. Chen and Y. Liu, Appl. Opt. 51, 457–464 (2012).
[20] A. Biswas and J. Coupland, Appl. Opt. 47, 1705–1710 (2008).
[21] L. Zhang, C. Tian, D. Liu, T. Shi, Y. Yang, et al. Appl. Opt. 53, 5755–5762 (2014).
[22] W. Sun, J. W. McBridge and M. Hill, Precis. Eng. 34, 171–179 (2010).
[23] N. El-Hayeka, H. Nouiraa, N. Anwer, O. Gibaru and M. Damak, Precis. Eng. 38, 935–947 (2014).
[24] S. DeFisher, G. Matthews and E. Fess, Proc. SPIE 9633, 96331M (2015).
[25] J. Yao, D. Xu, N. Zhao and J. P. Rolland, Proc. SPIE 9633, 96331A (2015).
[26] R. Kingslake, 'Lens Design Fundamentals. Second edition', (Academic Press, NY, 2010) Chapter 2, p. 46.
[27] S. R. Uhlhorn, D. Borja, F. Manns and J. Pare, Vision Res. 48, 2732–2738 (2008).
[28] B. E. A. Saleh and M. C. Teich, 'Fundamentals of Photonics', (John Wiley & Sons, New York, 1991).
[29] R. Huber, M. Wojtkowski and J. G. Fujimoto, Opt. Express 14, 3225–3237 (2006).